Research Square

Preprints are preliminary reports that have not undergone peer review.
They should not be considered conclusive, used to inform clinical practice,
or referenced by the media as validated information.

FCC vs. BCC Competition in Al–Fe–Ni–X Medium-Entropy Alloys: The Role of Ni Enrichment and Electronic Structure

Karla Y. Medrano-Zamudio
Universidad Michoacana de San Nicolás de Hidalgo
Hongbo Liu
Instituto Mexicano del Petróleo
Georgina Carbajal-De la Torre
Universidad Michoacana de San Nicolás de Hidalgo
Arnoldo Bedolla-Jacuinde
Universidad Michoacana de San Nicolás de Hidalgo
Marco Antonio Espinosa-Medina
maresmed@gmail.com
Universidad Michoacana de San Nicolás de Hidalgo

Research Article

Keywords: Medium-entropy alloys, FCC–BCC phase stability, Ni enrichment, Density functional theory, Electronic structure, Density of states

Posted Date: November 12th, 2026

DOI: https://doi.org/10.21203/rs.3.rs-11473784/v1

License: This work is licensed under a Creative Commons Attribution 4.0 International License.
Read Full License

Additional Declarations: No competing interests reported.

FCC vs. BCC Competition in Al–Fe–Ni–X Medium-Entropy Alloys: The Role of Ni Enrichment and Electronic Structure

K. Y. Medrano-Zamudio[1], Hongbo Liu[2,a], G. Carbajal-De la Torre[1], A. Bedolla-Jacuinde[3], and M. A. Espinosa-Medina[1,b]

[1] Facultad de Ingeniería Mecánica, Universidad Michoacana de San Nicolás de Hidalgo, C.P. 58000, Morelia, México

[2] Instituto Mexicano del Petróleo, C.P. 07730, Cd. de México, México

[3] Instituto de Investigación en Metalurgia y Materiales, Universidad Michoacana de San Nicolás de Hidalgo, C.P. 58000, Morelia, México

corresponding authors: [a] hbliu@imp.mx; [b] marespmed@gmail.com

Abstract

This study investigates energetic competition between face-centered cubic (FCC) and body-centered cubic (BCC) configurations in Al–Fe–Ni–X (X = Cr, Co, Mn) medium-entropy alloys upon Ni enrichment, using representative 16-atom FCC/BCC supercells compared by density functional theory. Ni enrichment does not produce a universal FCC-stabilizing response: for the Cr family, the FCC–BCC energy difference increases from +35.48 to +73.48 meV atom^{-1} (a shift of +38.00 meV atom^{-1} toward BCC), whereas the Co and Mn families decrease from +148.36 to +89.11 and from +111.96 to +84.73 meV atom^{-1}, respectively (shifts of −59.25 and −27.23 meV atom^{-1} toward FCC), although BCC remains the lowest-energy configuration in all six compositions. These energetic trends are accompanied by element- and structure-dependent changes in the d-character density of states near the Fermi level, most pronounced for Co, and by chemistry-dependent Mulliken charge redistribution between Al and the transition-metal sublattice. Structural analysis reveals a measurable BCC lattice distortion upon Ni enrichment, together with opposite volumetric responses in the two structures (BCC expansion of 5.7–10.1%, FCC contraction of 2.5–5.6%). Overall, FCC–BCC competition in Al–Fe–Ni–X alloys cannot be captured by a single descriptor such as VEC, but instead reflects a chemically specific reorganization of the electronic structure.

Keywords: Medium-entropy alloys; FCC–BCC phase stability; Ni enrichment; Density functional theory; Electronic structure; Density of states

1. Introduction

Medium-entropy alloys (MEAs) are multicomponent metallic systems in which several principal elements contribute significantly to their thermodynamic, structural, and electronic properties. Unlike conventional alloys, their phase constitution can be strongly affected by relatively small changes in composition, making the competition between face-centered cubic (FCC) and body-centered cubic (BCC) structures an important issue in the design of multicomponent alloys.

Al- and transition-metal-containing MEAs are particularly suitable for studying this competition because their phase stability is highly composition-dependent. For example, the $AlCrFe_2Ni_2$ alloy has been reported to exhibit an FCC phase together with disordered A2 and ordered B2 BCC phases [1]. Thermodynamic studies of the Al–Co–Cr–Fe–Ni system have likewise demonstrated that the relative stability of FCC-A1, BCC-A2, and BCC-B2 phases depends strongly on both composition and temperature [2]. First-principles calculations for equiatomic AlCrFeNi have further shown that FCC and BCC configurations can exhibit significant differences in energetic stability and electronic properties [3]. These studies demonstrate that the FCC–BCC competition in Al-containing multicomponent alloys cannot be described solely in terms of a single structural or thermodynamic parameter.

Several empirical descriptors have therefore been proposed to evaluate phase-formation tendencies in multicomponent alloys. Parameters such as mixing enthalpy, atomic-size difference, configurational entropy, electronegativity difference, and the Ω parameter are commonly used to assess the tendency toward solid-solution formation [4–7]. Among these descriptors, the valence electron concentration (VEC) has shown a particularly useful correlation with the tendency toward FCC or BCC structures [5]. Nevertheless, such criteria are primarily screening tools. They provide information about compositional tendencies but do not directly reveal how changes in chemical composition modify the electronic structure and energetic competition between different crystal structures.

Density functional theory (DFT) provides a means of addressing this limitation by enabling the direct comparison of different crystal configurations at a given composition and by providing access to their electronic structures. Comparison of the total and partial densities of states can provide information on how the electronic states associated with competing structures are reorganized when the alloy composition is modified. Such an approach is especially relevant for

transition-metal-containing alloys, where the partially occupied d states play an important role in determining bonding and structural stability. DFT-based studies of related Al-containing and Fe–Cr–Ni-based systems have shown that FCC and BCC configurations can differ measurably in relative energetic stability and electronic structure, further supporting the relevance of this approach for Al–Fe–Ni–X alloys [8–11].

Despite the established relationship between composition, VEC, and FCC/BCC tendencies, the extent to which a specific compositional modification produces a common energetic response across chemically different alloy families, and whether this response is accompanied by a universal electronic signature, remains less clear. Ni is of particular interest because increasing its concentration can substantially modify the VEC and the balance between FCC- and BCC-favoring elements. A systematic comparison of Ni enrichment in otherwise related Al–Fe–Ni–X systems can therefore help distinguish general compositional effects from electronic responses that depend on the identity of the fourth element.

In this work, Al–Fe–Ni–X medium-entropy alloys, where X = Cr, Co, and Mn, are investigated using a combined thermodynamic-screening and DFT approach. The three alloy families share the same Al–Fe–Ni chemical base, allowing the effect of the fourth element to be examined under a consistent compositional framework. For each family, equiatomic and Ni-enriched compositions are compared using representative 16-atom FCC and BCC supercells with identical effective compositions. The relative energetic stability of the two structures is evaluated from their binding energies extrapolated to zero electronic temperature, while the total density of states and d-character contribution near the Fermi level are analyzed to characterize the associated electronic changes.

The main objective is to determine how Ni enrichment modifies the relative FCC–BCC energetic stability across the three alloy families and whether the resulting energetic response is common or chemically dependent. By comparing Cr-, Co-, and Mn-containing systems within the same Al–Fe–Ni framework, this study seeks to distinguish general compositional effects from electronic responses associated with the identity of the fourth alloying element.

2. Methodology

2.1 Compositional Screening and Selection

Quaternary Al–Fe–Ni–X medium-entropy alloys, with X = Cr, Co, and Mn, were considered. A preliminary compositional screening was performed to identify representative compositions for subsequent first-principles calculations. The screening included equiatomic compositions as well as compositions enriched in selected constituent elements.

For each composition, the valence electron concentration (VEC), mixing enthalpy (ΔH_{mix}), configurational mixing entropy (ΔS_{mix}), mixing free energy (ΔG_{mix}), atomic-size difference (δ), Ω parameter, electronegativity difference ($\Delta\chi$), and theoretical density were evaluated. These quantities were used as empirical descriptors of solid-solution formation and the expected FCC/BCC structural tendency, following previously reported criteria for multicomponent alloys [4–7].

The configurational entropy was estimated assuming an ideal random solution. The mixing enthalpy was calculated from the binary interactions between the constituent elements, and the mixing free energy was obtained from the enthalpic and entropic contributions. The Ω parameter was considered together with the atomic-size difference δ as an empirical criterion for solid-solution formation, whereas VEC was used as a descriptor of the relative tendency toward FCC or BCC structures.

Six representative compositions were selected for the DFT calculations: AlFeNiCr, AlFeNiCo, AlFeNiMn, $AlFeNi_2Cr$, $AlFeNi_2Co$, and $AlFeNi_2Mn$. These compositions form three controlled pairs in which the effect of Ni enrichment can be evaluated for X = Cr, Co, and Mn while maintaining the same Al–Fe–Ni chemical framework.

2.2 Supercell Construction and Model Design

For each selected composition, representative FCC and BCC configurations were constructed using 16-atom supercells. The corresponding FCC/BCC models were designed to contain the same total number of atoms and the same effective chemical composition, allowing their energetic differences to be associated with the crystal structure rather than with differences in stoichiometry.

The equiatomic compositions AlFeNiCr, AlFeNiCo, and AlFeNiMn were represented by $Al_4Fe_4Ni_4Cr_4$, $Al_4Fe_4Ni_4Co_4$, and $Al_4Fe_4Ni_4Mn_4$, respectively. The Ni-enriched compositions were represented by $Al_3Fe_3Ni_7Cr_3$, $Al_3Fe_3Ni_7Co_3$, and $Al_3Fe_3Ni_7Mn_3$.

The atomic arrangements were not assigned arbitrarily. For the BCC-based configurations, the initial distribution of the constituent species was guided by experimentally reported site-occupation

and elemental-partitioning tendencies in chemically related Al–Fe–Ni–Cr–Co alloys. Combined neutron and X-Ray diffraction refinements of AlCoCrFeNi have shown preferential occupation of one B2 sublattice by Co and Ni and of the complementary sublattice by Al and Fe, whereas Cr exhibits no pronounced site preference [12]. Complementary experimental investigations using STEM/EDS, EPMA, and related microstructural characterization have reported Al–Ni-rich and Fe–Cr-rich chemical partitioning associated with BCC/B2 microstructures in Al-containing Co–Cr–Fe–Ni alloys [2,12–14]. These experimentally observed chemical tendencies were used as qualitative constraints when constructing the representative BCC models, while preserving the target composition of each 16-atom supercell.

For the FCC configurations, which were treated as substitutional A1-type structures with crystallographically equivalent lattice sites, the atomic species were distributed as homogeneously as possible throughout the supercell while avoiding artificial short-range clustering. For the Mn-containing models, for which no element-specific experimental site preference was imposed, the atomic species were distributed using the same homogeneous-construction criterion while avoiding artificial short-range clustering.

For each composition, the corresponding FCC and BCC models contained the same total number of atoms and identical effective chemical compositions. Accordingly, the energetic differences obtained for each FCC/BCC pair reflect the response of two consistently constructed representative configurations rather than differences in stoichiometry, as shown in Figure 1. Because only one 16-atom chemical configuration was considered for each structure and composition, the present models should not be interpreted as configurational averages equivalent to special quasirandom structures (SQS) [15], but rather as literature-informed representative configurations designed for controlled comparative analysis.

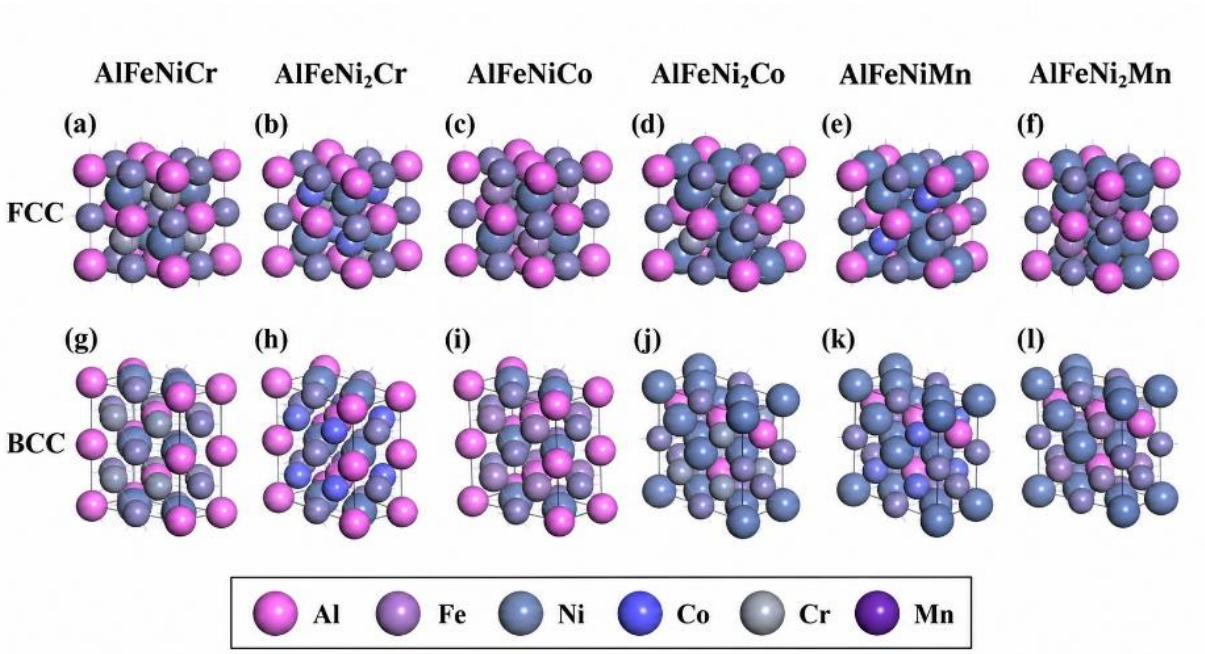


Fig.1 Representative 16-atom FCC (a–f) and BCC (g–l) supercells used in the DFT calculations for AlFeNiCr, AlFeNi$_2$Cr, AlFeNiCo, AlFeNi$_2$Co, AlFeNiMn, and AlFeNi$_2$Mn. The configurations preserve identical effective compositions within each FCC/BCC pair and were constructed using literature-informed elemental-distribution criteria. Color code: Al, pink; Fe, purple; Ni, grayish blue; Co, cobalt blue; Cr, gray; Mn, deep purple

2.3 Density functional theory calculations

First-principles calculations were performed within the framework of density functional theory (DFT) using the DMol^3 module implemented in Materials Studio 2017 (BIOVIA). Exchange–correlation effects were described using the generalized gradient approximation (GGA) with the Perdew–Burke–Ernzerhof (PBE) functional [16]. A DND numerical basis set and DSPP pseudopotentials were employed, together with a spin-unrestricted electronic treatment. The global orbital cutoff radius was set to 4.4 Å.

For each model, geometry optimization was initially performed by allowing both the atomic positions and the cell parameters to relax. Brillouin-zone integrations were carried out using Monkhorst–Pack *k*-point meshes [17] of 2 × 2 × 2 for the BCC supercells and 2 × 2 × 3 for the FCC supercells, considering the different dimensions of the representative cells. The self-consistent-field (SCF) electronic convergence criterion was set to 1.0 $\times 10^{-6}$. Geometry optimization was considered converged when the total-energy change between successive

optimization steps was below 1.0×10^{-5} Ha, the maximum atomic force was below 2.0×10^{-3} Ha $Å^{-1}$, the maximum atomic displacement was below 5.0×10^{-3} Å, and the SCF density-convergence criterion (1.0×10^{-6}) was satisfied; full cell-parameter (lattice) optimization was enabled throughout, with a maximum trial displacement of 0.3 Å per step.

Because the investigated systems are metallic and contain partially occupied electronic states near the Fermi level, thermal smearing was employed to improve SCF stability and convergence. A common thermal smearing value of 0.05 Ha was applied to the single-point calculations used for the FCC–BCC comparison to ensure a consistent treatment of partially occupied metallic states across all compositions and structures. The smearing parameter was employed exclusively as a numerical convergence aid and was not interpreted as a physical temperature or as a direct descriptor of phase stability [18, 19]. Geometry optimizations were performed using a smaller thermal smearing of 0.005 Ha to promote numerically stable structural relaxation; the larger, common value of 0.05 Ha was applied only in the subsequent single-point calculations used for the FCC–BCC energetic comparison (Section 2.4), consistently across all six compositions and both crystal structures. A *k*-point convergence check performed for the AlFeNiCo-FCC configuration, comparing 2 × 2 × 3 and 3 × 3 × 6 Monkhorst–Pack meshes, showed a change in the extrapolated binding energy of less than 0.5 meV $atom^{-1}$, supporting the adequacy of the *k*-point sampling adopted for the production calculations; this check was performed for a single representative composition and was not repeated systematically across the full set.

Following geometry optimization, single-point energy calculations were performed using the same PBE functional, DND basis set, DSPP pseudopotentials, spin-unrestricted treatment, global orbital cutoff radius of 4.4 Å, and a common thermal smearing value of 0.05 Ha. The relative energetic stability of the FCC and BCC configurations was evaluated using the binding energy extrapolated to zero electronic temperature as reported by DMol³.

The total density of states (TDOS) and the partial density of states associated with d-character states (d-DOS) were subsequently analyzed to examine the electronic changes accompanying the FCC–BCC energetic competition. The energy scale was referenced to the Fermi level, defined as $E_F = 0$ eV. The detailed numerical conditions employed for the DOS calculations were kept consistent within each comparison and are discussed together with the corresponding electronic-structure results.

2.4 Evaluation of relative FCC–BCC energetic stability

The relative energetic stability of the FCC and BCC configurations was evaluated using the binding energy extrapolated to zero electronic temperature, as reported by DMol[3]. For each composition, the energy difference per atom was defined as

$$\Delta E_{\mathrm{FCC-BCC}} = \frac{E_{\mathrm{FCC}}^{T=0} - E_{\mathrm{BCC}}^{T=0}}{N}, \quad (1)$$

where $E_{\mathrm{FCC}}^{T=0}$ and $E_{\mathrm{BCC}}^{T=0}$ are the corresponding binding energies extrapolated to zero electronic temperature and N is the total number of atoms in the supercell.

Because each FCC/BCC pair contains the same number of atoms and the same effective chemical composition, the contributions from the corresponding isolated constituent atoms are identical and cancel in the energy difference.

Under this definition, $\Delta E_{\mathrm{FCC-BCC}} < 0$ indicates that the FCC configuration has a lower calculated energy than the corresponding BCC configuration, whereas $\Delta E_{\mathrm{FCC-BCC}} > 0$ indicates a lower energy for the BCC configuration. Values close to zero indicate near-degenerate energetic competition between the two representative configurations.

To quantify the effect of Ni enrichment, the change in the FCC–BCC energy difference was defined as:

$$\Delta\Delta E_{\mathrm{Ni}} = \Delta E_{\mathrm{FCC-BCC}}^{\mathrm{Ni-enriched}} - \Delta E_{\mathrm{FCC-BCC}}^{\mathrm{equiatomic}}. \quad (2)$$

A negative $\Delta\Delta E_{\mathrm{Ni}}$ therefore indicates that Ni enrichment shifts the relative energetic competition toward FCC, whereas a positive value indicates a shift toward BCC.

The energetic results were subsequently analyzed together with the TDOS and d-DOS to determine whether the composition-dependent effect of Ni enrichment on the FCC–BCC energetic competition is accompanied by corresponding changes in the electronic structure.

3. Results and discussion

3.1. Thermodynamic screening and selection of representative compositions

A preliminary compositional screening of the Al–Fe–Ni–X systems, where X = Cr, Co, and Mn, was carried out to select representative compositions for the subsequent DFT analysis. The compositional space considered included the equiatomic AlFeNiX alloys and variants enriched in their constituent elements. For each composition, the valence electron concentration (VEC),

mixing enthalpy (ΔH_{mix}), configurational mixing entropy (ΔS_{mix}), mixing free energy (ΔG_{mix}), atomic-size difference (δ), Ω parameter, electronegativity difference ($\Delta\chi$), and theoretical density were evaluated. The combined use of thermodynamic, electronic, and atomic-mismatch parameters is a widely adopted strategy for assessing solid-solution formation tendencies and structural stability in multicomponent systems [4–7].

From this compositional space, six representative alloys were selected for further study: AlFeNiCr, AlFeNiCo, AlFeNiMn, $AlFeNi_2Cr$, $AlFeNi_2Co$, $AlFeNi_2Mn$. (Table 1).

Table 1. Screening parameters of the compositions selected for DFT

Composition	VEC	ΔH_{mix} (kJ/mol)	ΔS_{mix} (J/mol·K)	ΔG_{mix} (kJ/mol)	δ (%)	Ω	$\Delta\chi$	Density (g/cm³)	Structural tendency	Solid solution	Segregation	Intermetallic risk
AlFeNiCr	6.75	−11.25	11.53	−14.40	5.75	1.70	0.122	6.26	BCC/B2	Favorable	Moderate	Low
$AlFeNi_2Cr$	7.40	−11.04	11.08	−14.07	5.55	1.68	0.126	6.73	FCC+BCC	Favorable	Moderate	Low
AlFeNiCo	7.50	−13.50	11.53	−16.65	6.04	1.33	0.118	6.62	FCC+BCC	Favorable	Low	Low
$AlFeNi_2Co$	8.00	−12.48	11.08	−15.51	5.71	1.41	0.113	7.03	FCC	Favorable	Low	Low
AlFeNiMn	7.00	−13.50	11.53	−16.65	5.83	1.28	0.149	6.30	FCC+BCC	Favorable	Moderate	Low
$AlFeNi_2Mn$	7.60	−12.48	11.08	−15.51	5.59	1.37	0.153	6.75	FCC+BCC	Favorable	Moderate	Low

The selection strategy made it possible to retain the three equiatomic compositions as a reference and to compare them directly with their corresponding Ni-enriched variants. In this way, three controlled compositional series were established: Cr, Co, and Mn.

The selected compositions present δ values between 5.55% and 6.04% and Ω values between 1.28 and 1.70. These ranges satisfy the empirical criterion $\Omega \geq 1.1$ and $\delta \leq 6.6\%$ proposed by Yang and Zhang to favor the formation of multicomponent solid solutions [6]. However, these parameters were used exclusively as screening criteria and not as a definitive determination of phase stability, given that the structural constitution of multicomponent systems depends simultaneously on thermodynamic, chemical, and electronic contributions [4, 7].

VEC made it possible to identify particularly relevant trends among the selected families. In the Cr system, the increase in Ni raised VEC from 6.75 for AlFeNiCr to 7.40 for $AlFeNi_2Cr$, accompanied by a change in the estimated structural tendency from BCC/B2 to FCC+BCC. For the Co family, VEC increased from 7.50 to 8.00 and the estimated tendency evolved from FCC+BCC to FCC. In the Mn family, Ni enrichment increased VEC from 7.00 to 7.60, although both compositions remained within the estimated FCC+BCC region.

These observations are qualitatively consistent with the use of VEC as an empirical descriptor of the FCC/BCC competition [5]. However, the screening alone does not make it possible to determine the magnitude of the energetic preference between the two configurations, nor to identify the accompanying electronic response.

Therefore, the selection of the six compositions was not based solely on their potential to form solid solutions. The set was designed to address a specific question: to determine how Ni enrichment modifies the energetic competition between FCC and BCC configurations and whether the magnitude and direction of this effect depend on the chemical nature of the fourth element.

3.2. FCC–BCC energetic competition and effect of Ni enrichment

The relative energetic stability of the FCC and BCC configurations was evaluated using $\Delta E_0^{\mathrm{FCC-BCC}}$, calculated from the binding energies extrapolated to zero electronic temperature and normalized per atom. Because each FCC/BCC pair contains the same number of atoms and the same effective chemical composition, positive values indicate a lower calculated energy for the BCC configuration, whereas negative values indicate a lower energy for FCC.

Table 2. Relative energetic stability of the FCC and BCC configurations and effect of Ni enrichment.

Family	Composition	$\Delta E_0^{\mathrm{FCC-BCC}}$ (meV atom^{-1})	Preference	$\Delta\Delta E_{\mathrm{Ni}}$ (meV atom^{-1})
Cr	AlFeNiCr	35.48	BCC	—
Cr	$AlFeNi_2Cr$	73.48	BCC	38.00
Co	AlFeNiCo	148.36	BCC	—
Co	$AlFeNi_2Co$	89.11	BCC	−59.25
Mn	AlFeNiMn	111.96	BCC	—
Mn	$AlFeNi_2Mn$	84.73	BCC	−27.23

Note: $\Delta E_0^{\mathrm{FCC-BCC}} = E_{\mathrm{FCC}}^{T=0} - E_{\mathrm{BCC}}^{T=0}$. Positive values indicate a lower calculated energy for BCC, whereas negative values indicate a lower calculated energy for FCC. $\Delta\Delta E_{\mathrm{Ni}} = \Delta E_{0,\mathrm{Ni\ rich}}^{\mathrm{FCC-BCC}} - \Delta E_{0,\mathrm{equiatomic}}^{\mathrm{FCC-BCC}}$; therefore, negative values indicate a relative shift toward FCC and positive values a relative shift toward BCC.

The results show that the FCC–BCC energetic competition depends both on the chemical identity of the fourth element and on the Ni content. The calculated values of $\Delta E_0^{\mathrm{FCC-BCC}}$ and $\Delta\Delta E_{\mathrm{Ni}}$ are summarized in Table 2. Under the common numerical treatment employed in the present calculations, all six representative compositions exhibit positive $\Delta E_0^{\mathrm{FCC-BCC}}$ values, indicating that

the BCC configuration has the lower calculated energy within the representative models considered.

For the equiatomic compositions, $\Delta E_0^{\mathrm{FCC-BCC}}$ is +35.48 meV atom^{-1} for AlFeNiCr, +148.36 meV atom^{-1} for AlFeNiCo, and +111.96 meV atom^{-1} for AlFeNiMn. Thus, although BCC is energetically favored in all three systems, the magnitude of the FCC–BCC energetic separation is strongly dependent on the identity of the fourth element. The Cr-containing composition exhibits the smallest separation between the competing configurations, whereas the Co-containing system shows the largest BCC energetic advantage among the equiatomic alloys.

Ni enrichment produces an element-dependent response rather than a universal shift in the FCC–BCC energetic competition. In the Cr-containing family, $\Delta E_0^{\mathrm{FCC-BCC}}$ increases from +35.48 to +73.48 meV atom^{-1}, corresponding to $\Delta\Delta E_{\mathrm{Ni}}$ = +38.00 meV atom^{-1}. Within the representative configurations considered, Ni enrichment therefore increases the energetic separation in favor of BCC in the Cr-containing system.

An opposite trend is observed in the Co- and Mn-containing families. For Co, $\Delta E_0^{\mathrm{FCC-BCC}}$ decreases from +148.36 to +89.11 meV atom^{-1}, corresponding to $\Delta\Delta E_{\mathrm{Ni}}$ = −59.25 meV atom^{-1}. For Mn, the energetic difference decreases from +111.96 to +84.73 meV atom^{-1}, giving $\Delta\Delta E_{\mathrm{Ni}}$ = −27.23 meV atom^{-1}. The negative values indicate that increasing the Ni content shifts the relative energetic competition toward FCC in the Co- and Mn-containing systems, although the BCC configurations remain lower in calculated energy for the compositions investigated.

The magnitude and direction of the Ni-induced change are therefore chemically specific. The Co-containing family exhibits the strongest relative shift toward FCC, followed by Mn, whereas the Cr-containing family responds in the opposite direction. These results indicate that the influence of Ni on FCC–BCC energetic competition cannot be described as a universal FCC-stabilizing effect within the present Al–Fe–Ni–X series. Instead, its effect depends on the chemical environment established by the fourth alloying element.

This behavior is particularly relevant when compared with the compositional screening. Increasing Ni raises the VEC in all three families and, according to the empirical screening criteria, generally increases the expected tendency toward FCC-containing structures. However, the DFT calculations show that the corresponding energetic response is not universal, especially in the Cr-containing family. This difference emphasizes the role of VEC as a useful first-order screening descriptor rather than a definitive predictor of FCC–BCC energetic stability. The observed element-dependent

response therefore motivates a closer examination of the electronic structure to identify how Ni enrichment modifies the electronic states of the competing FCC and BCC configurations.

3.3. Electronic response of the relative FCC–BCC stability

The energetic results reveal that the effect of Ni enrichment on the FCC–BCC competition is strongly dependent on the chemical identity of the fourth alloying element. Although all representative configurations investigated in the present work remain energetically biased toward BCC, Ni enrichment modifies the magnitude of this preference in different directions. For the Cr-containing family, $\Delta E_0^{\mathrm{FCC-BCC}}$ increases from +35.48 to +73.48 meV atom^{-1}, corresponding to $\Delta\Delta E_{\mathrm{Ni}}$ =+38.00 meV atom^{-1}. Thus, within the representative configurations considered, Ni enrichment increases the relative energetic preference for BCC. In contrast, the Co- and Mn-containing families exhibit decreases in $\Delta E_0^{\mathrm{FCC-BCC}}$, from +148.36 to +89.11 meV atom^{-1} and from +111.96 to +84.73 meV atom^{-1}, respectively. These changes correspond to $\Delta\Delta E_{\mathrm{Ni}}$ =−59.25 meV atom^{-1} for Co and −27.23 meV atom^{-1} for Mn, indicating relative shifts toward FCC, although the BCC configurations remain lower in calculated energy for both compositions (Fig. 2a).

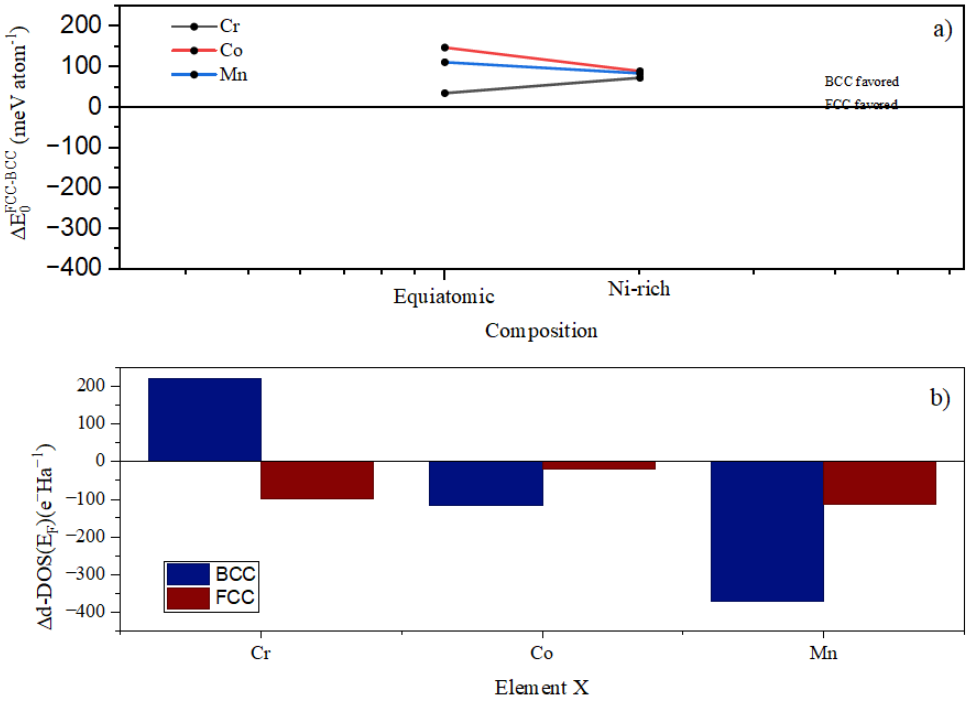


Fig.2 Effect of Ni enrichment on (a) the relative FCC–BCC stability and (b) the change in d-DOS at E_{F} for Al–Fe–Ni–X (X = Cr, Co and Mn)

To examine whether these composition-dependent energetic responses are accompanied by corresponding changes in electronic structure, the d-character density of states at the Fermi level, $\mathrm{d}-\mathrm{DOS}(E_\mathrm{F})$ was compared between the equiatomic and Ni-rich configurations. The electronic response was quantified as:

$$\Delta\mathrm{d}-\mathrm{DOS}(E_\mathrm{F}) = \mathrm{d}-\mathrm{DOS}_{\mathrm{Ni\ rich}}(E_\mathrm{F}) - \mathrm{d}-\mathrm{DOS}_{\mathrm{equiatomic}}(E_\mathrm{F}) \quad (3)$$

As shown in Fig. 2b, the response at the Fermi level depends strongly on both alloy chemistry and crystal structure. In the Cr-containing family, Ni enrichment produces a pronounced increase in the BCC d-DOS at E_F, with $\Delta\mathrm{d}-\mathrm{DOS}(E_\mathrm{F})$ =+8.12 $\mathrm{electrons\,eV^{-1}}$, whereas the FCC configuration exhibits a decrease of −3.64 $\mathrm{electrons\,eV^{-1}}$. This opposite response of the two competing structures accompanies the relative energetic shift toward BCC observed for the Cr-containing system.

The Co- and Mn-containing families exhibit a different electronic response. For Co, $\Delta\mathrm{d}-\mathrm{DOS}(E_\mathrm{F})$ decreases by −4.31 $\mathrm{electrons\,eV^{-1}}$, in BCC and by −0.75 $\mathrm{electrons\,eV^{-1}}$, in FCC. For Mn, the corresponding decreases are substantially larger, reaching −13.61 $\mathrm{electrons\,eV^{-1}}$, in BCC and −4.14 $\mathrm{electrons\,eV^{-1}}$, in FCC. Therefore, both Co and Mn show a reduction of d-character states at the Fermi level in the two crystal structures, with the largest change occurring in BCC. However, the magnitude of this electronic variation does not scale directly with the energetic response: Co exhibits the largest relative energetic shift toward FCC despite showing a considerably smaller reduction in BCC $\Delta\mathrm{d}-\mathrm{DOS}(E_\mathrm{F})$ than Mn. This result indicates that the pointwise density of states at the Fermi level cannot, by itself, serve as a quantitative predictor of the FCC–BCC energetic competition.

The Co-containing family was selected for a more detailed examination of the complete electronic spectra because it exhibits the largest Ni-induced energetic shift toward FCC among the three systems. Figure 3 compares the TDOS and $\mathrm{d}-\mathrm{DOS}$ of the BCC and FCC configurations for the equiatomic and Ni-rich Co-containing models. In the equiatomic composition, the BCC and FCC configurations exhibit clearly different distributions of electronic states in the occupied region below the Fermi level (Fig. 3a). The $\mathrm{d}-\mathrm{DOS}$ at E_F is approximately 9.27 $\mathrm{electrons\,eV^{-1}}$ for BCC and 5.71 $\mathrm{electrons\,eV^{-1}}$ for FCC, indicating a substantially larger contribution of d-character states at the Fermi level in the BCC configuration.

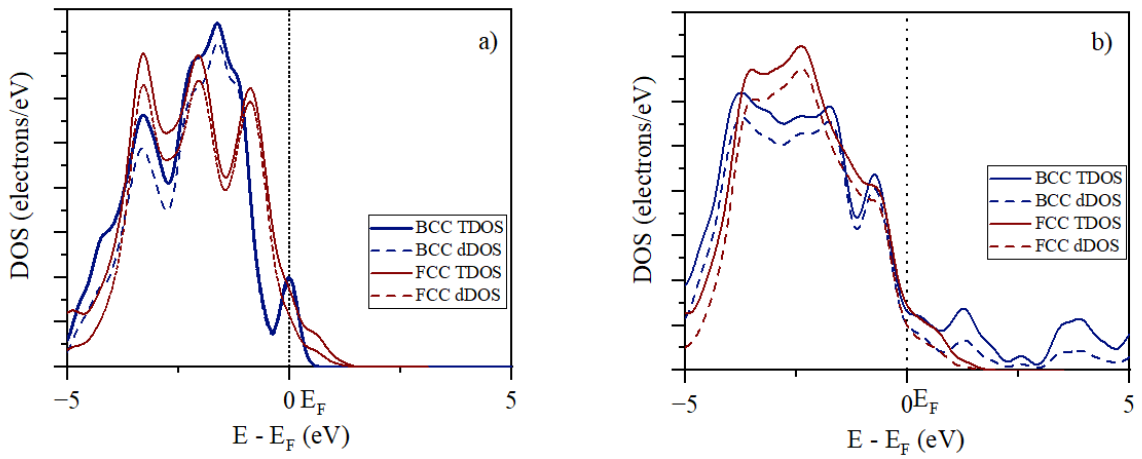


Fig.3 Total density of states (TDOS) and d-character density of states ($\mathrm{d-DOS}$) for the FCC and BCC configurations of (a) equiatomic AlFeNiCo and (b) Ni-enriched $AlFeNi_2Co$. Energies are referenced to the Fermi level (E_F = 0 eV)

Following Ni enrichment, the near-Fermi electronic structure of the two configurations becomes markedly modified (Fig. 3b). The BCC $\mathrm{d-DOS}$ at E_F decreases from 9.27 to 4.96 $\mathrm{electrons\ eV^{-1}}$, whereas the FCC value changes more moderately from 5.71 to 4.97 $\mathrm{electrons\ eV^{-1}}$. Consequently, the large difference between the BCC and FCC $\mathrm{d-DOS}$ at the Fermi level observed in the equiatomic alloy is strongly reduced in the Ni-rich composition. The complete DOS profiles further show that this modification is not restricted to the Fermi level but is accompanied by a redistribution of spectral weight over the occupied d-state region below the Fermi level E_F.

This differential response is consistent with the substantial reduction in the calculated FCC–BCC energy separation observed for the Co-containing family. However, the present results do not support a simple relationship in which either an increase or decrease in $\mathrm{d-DOS}(E_F)$ uniquely determines structural stability. Instead, the relative energy of the competing FCC and BCC configurations reflects the integrated electronic-energy balance associated with the redistribution and hybridization of occupied states over a broader energy range.

Because all calculations were performed within a spin-unrestricted framework, in which the α and β electron densities were allowed to differ freely, the resulting Mulliken spin populations provide a direct probe of the magnetic character of each relaxed configuration. Among the twelve representative configurations, the Mulliken spin populations are essentially zero for eleven models. The equiatomic AlFeNiCo BCC configuration is the only case exhibiting substantial spin

polarization, with local Mulliken moments of approximately −0.207, +2.708, +0.174, and +0.867 μ_B on Al, Fe, Ni, and Co, respectively, corresponding to a summed atomic Mulliken spin of approximately 14.17 μ_B per 16-atom cell. Because the AlFeNiCo family is also the system exhibiting the largest FCC–BCC energetic separation among the equiatomic compositions (Section 3.2), this magnetic asymmetry between the BCC and FCC configurations may constitute an additional contribution to their electronic differentiation. To test whether the near-zero spin populations obtained elsewhere reflect a genuine electronic ground state rather than an artifact of the default spin initialization — which seeds a spin perturbation on a single Al atom only — single-point calculations were repeated for the three equiatomic FCC configurations (AlFeNiCr, AlFeNiCo, AlFeNiMn) using explicit, atom-resolved initial spin densities based on Hund's-rule high-spin values for the free transition-metal atoms (Fe: 4 μ_B; Co: 3 μ_B; Ni: 2 μ_B; Cr: 5 μ_B; Mn: 5 μ_B). In all three cases, the seeded calculations converged back to Mulliken spin populations of essentially zero on every atom, with total energies differing from the original, unseeded results by less than 0.001 meV atom^{-1} — well within numerical noise. This indicates that the non-magnetic solution obtained for the equiatomic FCC configurations of Cr, Co, and Mn is robust to the choice of initial spin density. The corresponding equiatomic BCC configurations were not subjected to the same re-seeding test, with the exception of AlFeNiCo-BCC, whose spontaneous convergence to a spin-polarized solution already demonstrates that the default initialization is capable of locating a magnetic minimum when one exists. The six Ni-enriched compositions, and a genuinely antiferromagnetic (sign-alternated) spin configuration, were not tested in the present study and are identified as a remaining item for future verification.

Overall, as proposed in Fig. 4, the combined energetic and electronic analyses indicate that Ni enrichment does not induce a universal structural response in Al–Fe–Ni–X alloys. Instead, the response depends on the chemical identity of the fourth element and on the way in which Ni modifies the electronic states of the competing FCC and BCC configurations. Cr exhibits a relative shift toward BCC together with opposite changes in the near-Fermi d-states of the two structures, whereas Co and Mn show relative shifts toward FCC accompanied by reductions in $\mathrm{d}-\mathrm{DOS}(E_F)$ for both configurations. These results support a chemistry-dependent electronic response associated with the FCC–BCC energetic competition, in which Ni enrichment redistributes d−character states differently in each alloy family, accompanying the element-specific

modification of the FCC–BCC energetic balance rather than a single universal stabilization pathway.

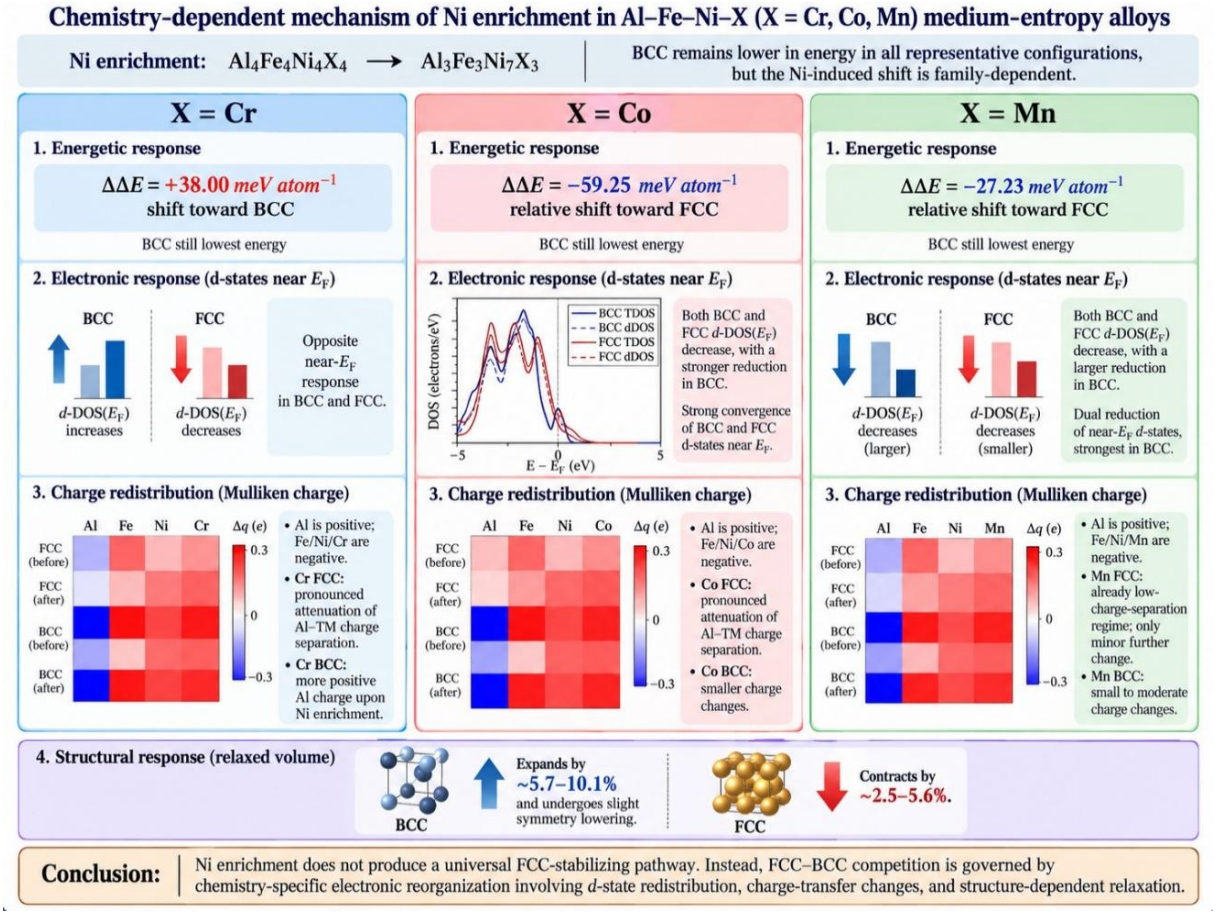


Fig. 4 Chemistry-dependent effects of Ni enrichment on FCC–BCC relative energetic stability and d-character density of states at the Fermi level in Al–Fe–Ni–X (X = Cr, Co, Mn). Values of $\Delta\Delta E_{Ni}$ are taken from Table 2; DOS trends are based on the calculated results described in Section 3.3.

3.4. Mulliken charge redistribution induced by Ni enrichment

To complement the energetic and density-of-states analyses, Mulliken population analysis was used to examine how Ni enrichment modifies the charge distribution among the constituent elements. In all investigated configurations, Al carries a positive average Mulliken charge, whereas Fe, Ni, and the fourth alloying element exhibit negative values, indicating a net redistribution of electronic density from Al toward the transition-metal sublattice. The magnitude of this charge separation, however, depends on both alloy chemistry and crystal structure.

In the equiatomic systems, the average Mulliken charge on Al ranges from approximately +1.35 to +1.47 e, while the transition metals carry negative charges whose magnitude varies with the identity of the fourth element. Cr exhibits the most negative q_X values, reaching approximately −0.70 e, followed by Co and Mn. The corresponding BCC and FCC configurations show relatively similar charge magnitudes for the Cr-containing family, whereas larger structure-dependent differences are observed for Co and Mn.

Ni enrichment produces a pronounced charge redistribution in the FCC configurations of the Cr- and Co-containing families: the average positive charge on Al decreases from +1.47 and +1.35 e in the equiatomic FCC models to +0.93 and +0.80 e, respectively, in the Ni-rich configurations, while Fe, Ni, and X become correspondingly less negative. The Mn-containing family follows a different pattern: the equiatomic AlFeNiMn FCC configuration already exhibits a comparatively small average Al charge (+0.845 e), close in magnitude to the Ni-rich value (+0.822 e), so that Ni enrichment produces only a marginal further change (−0.02 e) rather than the pronounced reduction observed for Cr and Co. Thus, Ni enrichment markedly reduces the magnitude of charge separation between Al and the transition-metal sublattice in the Cr and Co FCC systems, whereas the Mn-containing FCC system remains in a comparatively low-charge-separation regime at both compositions.

The BCC response is less uniform. In the Cr-containing family, the Al charge increases from +1.43 to +1.56 e, while the negative charges on Ni and Cr decrease in magnitude. In the Co-containing BCC configuration, the Al charge changes only slightly, whereas Ni and Co become substantially less negative and Fe becomes slightly more negative. The Mn-containing BCC system shows a comparatively moderate attenuation of the negative charges on Fe, Ni, and Mn, with almost no change in the average Al charge. These differences demonstrate that the redistribution induced by Ni enrichment is strongly dependent on the local chemical environment.

The contrast between the FCC and BCC responses is especially relevant when considered together with the energetic trends discussed above. The Cr- and Co-containing Ni-rich FCC configurations exhibit a pronounced reduction in the magnitude of Al-to-transition-metal charge separation, whereas the Mn-containing FCC configuration shows only a marginal further change, having already reached a comparatively low charge-separation regime in the equiatomic composition (above). The BCC configurations display element-dependent behavior instead: Cr, which exhibits a relative energetic shift toward BCC upon Ni enrichment, is also the only family in which the

BCC Al charge becomes markedly more positive, whereas Co and Mn, which shift relatively toward FCC, show a weaker or negligible increase in BCC Al charge.

These results suggest that the chemistry-dependent FCC–BCC energetic response is accompanied not only by changes in the near-Fermi d-states but also by a redistribution of charge between Al and the transition-metal sublattice. The Mulliken analysis should be interpreted comparatively rather than as an absolute measure of charge transfer, because population values depend on the chosen basis and partitioning scheme. Nevertheless, the consistent trends obtained within the same computational framework provide complementary evidence that Ni enrichment modifies the electronic environment differently in Cr-, Co-, and Mn-containing alloys.

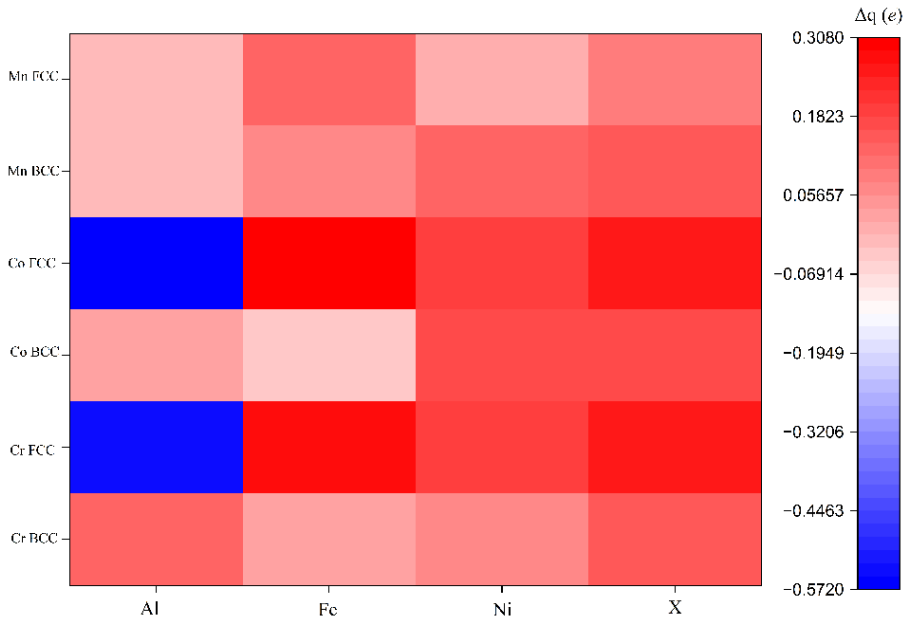


Fig.5 Heatmap of the change in average Mulliken charge induced by Ni enrichment in the BCC and FCC configurations of the Al–Fe–Ni–X systems (X = Cr, Co, and Mn). The charge variation is defined as $\Delta q_i = q_i^{\text{Ni rich}} - q_i^{\text{equiatomic}}$. Negative values indicate a decrease in the average Mulliken charge, whereas positive values indicate an increase

Figure 5 summarizes the Ni-induced Mulliken charge redistribution through the quantity for each atomic species in the BCC and FCC configurations. The heatmap highlights a structure-dependent response: the Cr- and Co-containing FCC systems exhibit a pronounced reduction in the positive Mulliken charge of Al together with a simultaneous decrease in the magnitude of the negative

charges carried by Fe, Ni, and X, indicating an attenuation of the Al-to-transition-metal charge separation upon Ni enrichment; the Mn-containing FCC system, in contrast, shows only a marginal change, having already reached a comparatively low charge-separation state in the equiatomic composition. In the BCC configurations, the Cr-containing system shows an increase in the positive Al charge, whereas the Co- and Mn-containing systems exhibit much smaller changes. Taken together with the energetic and DOS results, this behavior supports the interpretation that Ni enrichment modifies the electronic environment through an element- and structure-dependent redistribution of charge and d-character states, with the Mn-containing FCC system representing a distinct case in which the low-charge-separation regime is already present prior to Ni enrichment. The Mulliken analysis therefore provides complementary evidence that the FCC–BCC energetic response is not governed by a universal stabilization mechanism, but rather by the specific chemical environment established by the fourth alloying element.

To further characterize the chemical environment underlying these charge shifts, the mean Mulliken charge and the corresponding intra-configuration standard deviation were evaluated for each atomic species within each 16-atom supercell, $\sigma_i = \mathrm{std}(q_i)$ computed over all atoms of *i*-species present in a given configuration (Table 3). In the equiatomic compositions and in the Ni-enriched BCC configurations, this intra-configuration spread is small ($\sigma \leq 0.02$ e for the equiatomic systems, and ≤ 0.08 e for the Ni-enriched BCC cells), indicating that atoms of a given species occupy nearly equivalent local environments within these cells. In marked contrast, the Ni-enriched FCC configurations exhibit substantially larger standard deviations for Al, Fe and Ni (σ(Al) = 0.126 e for $AlFeNi_2Cr$-FCC, and 0.077–0.081 e for the Co- and Mn-containing Ni-rich FCC systems), showing that, within these single representative supercells, individual atoms of the same species carry appreciably different Mulliken charges depending on their specific local coordination. This intra-cell charge heterogeneity is most pronounced precisely in the Ni-rich FCC configurations that also show the largest reduction in average Al charge (above) and, for Co, the largest energetic shift toward FCC (Section 3.2), suggesting that Ni enrichment does not simply rescale the charge transfer uniformly but instead differentiates the local electronic environment among crystallographically distinct sites. This dispersion reflects variability among sites within a single 16-atom configuration; it is therefore complementary to, and not a substitute for, the configurational-sampling limitation discussed in the concluding remarks, and it does not by itself

quantify the uncertainty associated with the specific atomic arrangement chosen for each composition.

Table 3. Mean Mulliken charges and intra-configuration standard deviation (σ) per atomic species for the equiatomic and Ni-enriched BCC and FCC configurations.

Composition	Phase	$\bar{q}$(Al) (e)	σ(Al)	$\bar{q}$(Fe) (e)	σ(Fe)	$\bar{q}$(Ni) (e)	σ(Ni)	$\bar{q}$(X) (e)	σ(X)	X
AlFeNiCr	BCC	+1.434	0.000	−0.385	0.000	−0.349	0.000	−0.700	0.000	Cr
AlFeNiCr	FCC	+1.467	0.001	−0.419	0.001	−0.349	0.000	−0.699	0.000	Cr
AlFeNiCo	BCC	+1.398	0.000	−0.306	0.000	−0.419	0.000	−0.673	0.000	Co
AlFeNiCo	FCC	+1.355	0.001	−0.429	0.000	−0.337	0.000	−0.588	0.000	Co
AlFeNiMn	BCC	+1.472	0.000	−0.420	0.000	−0.403	0.000	−0.649	0.000	Mn
AlFeNiMn	FCC	+0.845	0.002	−0.264	0.002	−0.159	0.000	−0.422	0.000	Mn
$AlFeNi_2Cr$	BCC	+1.563	0.017	−0.370	0.047	−0.272	0.019	−0.558	0.000	Cr
$AlFeNi_2Cr$	FCC	+0.934	0.126	−0.141	0.084	−0.154	0.047	−0.434	0.144	Cr
$AlFeNi_2Co$	BCC	+1.424	0.018	−0.354	0.061	−0.242	0.079	−0.506	0.000	Co
$AlFeNi_2Co$	FCC	+0.796	0.077	−0.122	0.117	−0.150	0.057	−0.324	0.099	Co
$AlFeNi_2Mn$	BCC	+1.460	0.017	−0.350	0.066	−0.266	0.066	−0.490	<0.001	Mn
$AlFeNi_2Mn$	FCC	+0.822	0.081	−0.133	0.107	−0.154	0.051	−0.328	0.113	Mn

3.5. Structural response: lattice parameters and Ni-induced distortion

The geometry optimizations of the twelve representative FCC and BCC configurations were carried out under the convergence criteria specified in Section 2.3 (energy tolerance 1.0×10^{-5} Ha, maximum gradient 2.0×10^{-3} Ha Å^{-1}, maximum atomic displacement 5.0×10^{-3} Å, with lattice optimization enabled). Table 4 reports the resulting lattice parameters, cell angles, cell volume and volume per atom for each configuration.

Ni enrichment produces opposite volumetric responses in the two structural families. The relaxed BCC configurations expand by approximately 5.7–10.1%, whereas the corresponding FCC configurations contract by approximately 2.5–5.6%. In absolute terms, BCC V/atom increases from 11.60 to 12.62 Å³ (Cr family), from 11.64 to 12.31 Å³ (Co family), and from 11.31 to 12.45 Å³ (Mn family), while the corresponding FCC values decrease from 14.67 to 14.30 Å³ (Cr), 14.54 to 13.90 Å³ (Co), and 14.92 to 14.09 Å³ (Mn). Figure 6 illustrates this trend across the three families. This behavior indicates that Ni enrichment produces a measurable structural response in the relaxed cell dimensions, in addition to the energetic and electronic effects discussed in Sections 3.2–3.4.

Table 4. Optimized lattice parameters, cell angles, cell volume and volume per atom for the twelve representative BCC and FCC configurations.

Composition	Phase	*a* (Å)	*b* (Å)	*c* (Å)	*α* (°)	*β* (°)	*γ* (°)	*V* (Å³)	*V*/atom (Å³)
AlFeNiCr	BCC	5.70357	5.70357	5.70357	90.000	90.000	90.000	185.541	11.5963
AlFeNiCr	FCC	7.67796	7.99533	3.82332	90.000	90.000	90.000	234.706	14.6691
AlFeNiCo	BCC	5.71092	5.71092	5.71092	90.000	90.000	90.000	186.259	11.6412
AlFeNiCo	FCC	7.78621	7.67258	3.89532	90.000	90.000	90.000	232.708	14.5442
AlFeNiMn	BCC	5.65575	5.65575	5.65575	90.000	90.000	90.000	180.913	11.3071
AlFeNiMn	FCC	7.85112	7.75689	3.92038	90.000	90.000	90.000	238.752	14.9220
$AlFeNi_2Cr$	BCC	5.83728	5.83733	5.92825	89.976	89.976	89.771	201.999	12.6249
$AlFeNi_2Cr$	FCC	7.72947	7.69060	3.84883	90.000	90.000	89.187	228.768	14.2980
$AlFeNi_2Co$	BCC	5.74762	5.74764	5.96106	89.927	89.927	89.877	196.924	12.3078
$AlFeNi_2Co$	FCC	7.63413	7.64152	3.81205	90.000	90.000	89.245	222.362	13.8976
$AlFeNi_2Mn$	BCC	5.89939	5.81013	5.81015	89.866	90.000	90.000	199.149	12.4468
$AlFeNi_2Mn$	FCC	7.67955	7.66223	3.83151	90.000	90.000	89.219	225.434	14.0896

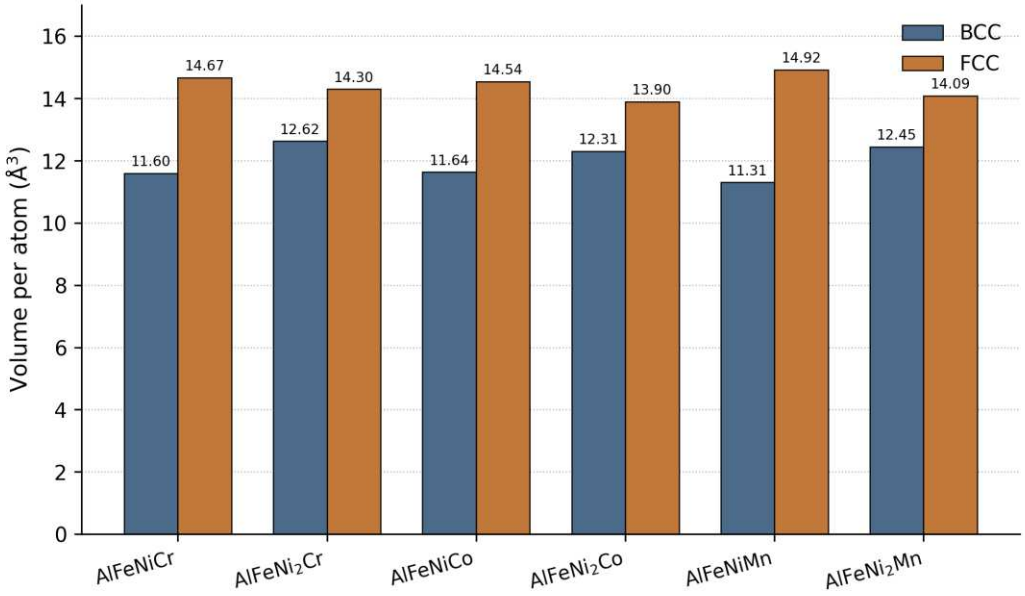


Fig.6 Volume per atom of the relaxed BCC and FCC configurations for the equiatomic and Ni-enriched Al–Fe–Ni–X (X = Cr, Co, Mn) compositions

A further structural feature emerges from the optimized geometries: the BCC configurations of the equiatomic compositions (AlFeNiCr, AlFeNiCo, AlFeNiMn) relax to an exactly cubic cell ($a = b = c$; $\alpha = \beta = \gamma = 90.000°$), whereas the BCC configurations of the Ni-enriched compositions

($AlFeNi_2Cr$, $AlFeNi_2Co$, $AlFeNi_2Mn$) relax to a lower-symmetry cell, with lattice vectors differing by up to ≈ 0.09 Å and cell angles deviating from 90° by up to ≈ 0.23° (e.g., γ = 89.771° for $AlFeNi_2Cr$, α = 89.927° for $AlFeNi_2Co$). This symmetry lowering was not imposed in the initial structure and emerges from unconstrained lattice optimization under tolerances well below the observed deviations, indicating a modest symmetry-lowering distortion within the representative Ni-enriched BCC configurations.

This structural response reinforces the chemically specific character of the Ni-enrichment effect discussed throughout Section 3: the same compositional change that shifts the FCC–BCC energetic balance (Section 3.2), redistributes near-Fermi d-states (Section 3.3), and broadens the intra-cell Mulliken charge distribution in FCC (Section 3.4) also perturbs the local lattice symmetry of the BCC phase. As with the other results presented here, this observation is based on a single representative configuration per composition; a systematic assessment of this distortion — for instance, using multiple atomic arrangements, full elastic-constant calculations, or group-theoretical mode analysis — was not performed in the present study and is identified as a direction for future work.

4. Conclusions

Density functional theory calculations using representative 16-atom configurations demonstrate that Ni enrichment modifies FCC–BCC energetic competition in Al–Fe–Ni–X (X = Cr, Co, Mn) medium-entropy alloys in a chemistry-dependent manner. BCC remains lower in calculated energy for all six compositions. However, Ni enrichment strengthens the relative BCC preference in the Cr family ($\Delta\Delta E_{Ni}$ = +38.00 meV atom^{-1}), whereas the Co and Mn families shift relatively toward FCC (−59.25 and −27.23 meV atom^{-1}, respectively), without reversing the energetic ordering.

These different energetic responses are accompanied by element- and structure-dependent changes in the d-character density of states near the Fermi level and in Mulliken charge distributions. The Co family shows the largest relative energetic shift toward FCC, although its near-Fermi d-DOS change is smaller than that of Mn, demonstrating that the DOS at a single energy is not a quantitative stability predictor. Ni enrichment also induces modest lower-symmetry distortions in the representative BCC cells, with BCC expansion and FCC contraction.

Thus, VEC is useful for preliminary compositional screening but does not determine the FCC–BCC energetic response by itself. The results support an interpretation involving composition-

specific electronic reorganization rather than a universal Ni-driven FCC-stabilization mechanism. These conclusions apply to the selected atomic configurations, not configurationally averaged phase equilibria. Further configurational sampling, including larger cells or special quasirandom structures, systematic magnetic-state testing, and species-resolved electronic analysis is needed to assess the robustness and microscopic origin of these trends.

Acknowledgments

The authors gratefully acknowledge the support provided by the Materials Degradation Laboratory of the Universidad Michoacana de San Nicolás de Hidalgo and the Instituto Mexicano del Petróleo. Financial support from the 2026 Research Project of the Coordination of Scientific Research of the Universidad Michoacana de San Nicolás de Hidalgo is also gratefully acknowledged.

Author Contributions

K. Y. Medrano Zamudio and **Hongbo Liu**: Conceptualization, Investigation, Methodology, Formal analysis, Writing - Original Draft. **G. Carbajal De la Torre** and **A. Bedolla Jacuinde**: Visualization, Supervision, Analysis, Writing – review & editing. **M. A. Espinosa Medina**: Analysis, Supervision, Project administration, Resources, Funding acquisition, Writing – review & editing.

Funding.

This research did not receive any specific grant from funding agencies in the public, commercial, or not-for-profit sectors.

Data availability

The data that support the findings of this study are available from the corresponding author upon reasonable request

Declaration of Competing Interest

The authors declare that they have no known competing financial interests or personal relationships that could have appeared to influence the work reported in this paper.

References

1. Dong Y, Gao X, Lu Y, Wang T, Li T (2016) A multi-component $AlCrFe_2Ni_2$ alloy with excellent mechanical properties. Mater Lett 169:62–64. https://doi.org/10.1016/j.matlet.2016.01.096
2. Stryzhyboroda O, Witusiewicz VT, Gein S, Röhrens D, Hecht U (2020) Phase equilibria in the Al–Co–Cr–Fe–Ni high entropy alloy system: thermodynamic description and experimental study. Front Mater 7:270. https://doi.org/10.3389/fmats.2020.00270
3. Wen Z, Zhao Y, Tian J, Wang S, Guo Q, Hou H (2019) Computation of stability, elasticity and thermodynamics in equiatomic AlCrFeNi medium-entropy alloys. J Mater Sci 54:2566–2576. https://doi.org/10.1007/s10853-018-2943-7
4. Zhang Y, Zhou YJ, Lin JP, Chen GL, Liaw PK (2008) Solid-solution phase formation rules for multi-component alloys. Adv Eng Mater 10:534–538. https://doi.org/10.1002/adem.200700240
5. Guo S, Ng C, Lu J, Liu CT (2011) Effect of valence electron concentration on stability of fcc or bcc phase in high entropy alloys. J Appl Phys 109:103505. https://doi.org/10.1063/1.3587228
6. Yang X, Zhang Y (2012) Prediction of high-entropy stabilized solid-solution in multi-component alloys. Mater Chem Phys 132:233–238. https://doi.org/10.1016/j.matchemphys.2011.11.021
7. Poletti MG, Battezzati L (2014) Electronic and thermodynamic criteria for the occurrence of high entropy alloys in metallic systems. Acta Mater 75:297–306. https://doi.org/10.1016/j.actamat.2014.04.033
8. Ogura M, Fukushima T, Zeller R, Dederichs PH (2017) Structure of the high-entropy alloy $Al_xCrFeCoNi$: fcc versus bcc. J Alloys Compd 715:454–459. https://doi.org/10.1016/j.jallcom.2017.04.318
9. Woodgate CD, Marchant GA, Pártay LB, Staunton JB (2024) Structure, short-range order, and phase stability of the $Al_xCrFeCoNi$ high-entropy alloy: insights from a perturbative, DFT-based analysis. npj Comput Mater 10:271. https://doi.org/10.1038/s41524-024-01445-w

10. Wróbel JS, Nguyen-Manh D, Lavrentiev MY, Muzyk M, Dudarev SL (2015) Phase stability of ternary fcc and bcc Fe–Cr–Ni alloys. Phys Rev B 91:024108. https://doi.org/10.1103/PhysRevB.91.024108
11. Fedorov M, Wróbel JS, Chromiński W, Cieślak G, Płocińska M, Kurzydłowski KJ, Nguyen-Manh D (2023) Composition stability of single fcc phase in Cr–Fe–Mn–Ni alloys: first-principles prediction and experimental validation. Acta Mater 255:119047. https://doi.org/10.1016/j.actamat.2023.119047
12. Karlsson D, Beran P, Riekehr L, Tseng JC, Harlin P, Jansson U, Cedervall J (2022) Structure and phase transformations in gas atomized AlCoCrFeNi high entropy alloy powders. J Alloys Compd 893:162060. https://doi.org/10.1016/j.jallcom.2021.162060
13. Li M, Gazquez J, Borisevich A, Mishra R, Flores KM (2018) Evaluation of microstructure and mechanical property variations in Al_xCoCrFeNi high entropy alloys produced by a high-throughput laser deposition method. Intermetallics 95:110–118. https://doi.org/10.1016/j.intermet.2018.01.021
14. Ma Y, Jiang B, Li C, Wang Q, Dong C, Liaw PK, Xu F, Sun L (2017) The BCC/B2 morphologies in Al_xNiCoFeCr high-entropy alloys. Metals 7:57. https://doi.org/10.3390/met7020057
15. Wei SH, Ferreira LG, Bernard JE, Zunger A (1990) Electronic properties of random alloys: special quasirandom structures. Phys Rev B 42:9622–9649. https://doi.org/10.1103/PhysRevB.42.9622
16. Perdew JP, Burke K, Ernzerhof M (1996) Generalized gradient approximation made simple. Phys Rev Lett 77:3865–3868. https://doi.org/10.1103/PhysRevLett.77.3865
17. Monkhorst HJ, Pack JD (1976) Special points for Brillouin-zone integrations. Phys Rev B 13:5188. https://doi.org/10.1103/PhysRevB.13.5188
18. Verstraete MJ, Gonze X (2004) Metals at finite temperature: a modified smearing scheme. Comput Mater Sci 30:27–33. https://doi.org/10.1016/j.commatsci.2004.01.006
19. Basiuk VA, Prezhdo OV, Basiuk EV (2020) Thermal smearing in DFT calculations: how small is really small? A case of La and Lu atoms adsorbed on graphene. Mater Today Commun 25:101595. https://doi.org/10.1016/j.mtcomm.2020.101595